



Article

Direct Synthesis of Dimethyl Ether from Syngas on Bifunctional Hybrid Catalysts Based on Supported $\text{H}_3\text{PW}_{12}\text{O}_{40}$ and Cu-ZnO(Al): Effect of Heteropolyacid Loading on Hybrid Structure and Catalytic Activity

Elena Millán , Noelia Mota, Rut Guil-López, Bárbara Pawelec , José L. García Fierro and Rufino M. Navarro *

Instituto de Catálisis y Petroleoquímica (CSIC), C/Marie Curie 2, Cantoblanco, 28049 Madrid, Spain; elena.millan.ordonez@csic.es (E.M.); noelia.mota@icp.csic.es (N.M.); rut.guil@icp.csic.es (R.G.-L.); bgarcia@icp.csic.es (B.P.); jlgfierro@icp.csic.es (J.L.G.F.)

* Correspondence: r.navarro@icp.csic.es

Received: 27 August 2020; Accepted: 15 September 2020; Published: 17 September 2020



Abstract: The performance of bifunctional hybrid catalysts based on phosphotungstic acid ($\text{H}_3\text{PW}_{12}\text{O}_{40}$, HPW) supported on TiO_2 combined with Cu-ZnO(Al) catalyst in the direct synthesis of dimethyl ether (DME) from syngas has been investigated. We studied the effect of the HPW loading on TiO_2 (from 1.4 to 2.7 monolayers) on the dispersion and acid characteristics of the HPW clusters. When the concentration of the heteropolyacid is slightly higher than the monolayer (1.4 monolayers) the acidity of the clusters is perturbed by the surface of titania, while for concentration higher than 1.7 monolayers results in the formation of three-dimensional HPW nanocrystals with acidity similar to the bulk heteropolyacid. Physical hybridization of supported heteropolyacids with the Cu-ZnO(Al) catalyst modifies both the acid characteristics of the supported heteropolyacids and the copper surface area of the Cu-ZnO(Al) catalyst. Hybridization gives rise to a decrease in the copper surface area and the disappearance of the strong acidic sites typical of HPW nanocrystals, showing all hybrids similar acid sites of weak or medium strength. The activity of the hybrids was tested for direct DME synthesis from syngas at 30 bar and 250 °C; only the hybrids with HPW loading higher than 1.4 monolayers showed activity for the direct synthesis of DME, showing that the sample loaded with 2.7 monolayers of heteropolyacid had higher activity than the reference hybrid representative of the most widely applied catalysts based on the combination of Cu-ZnO(Al) with HZSM-5. In spite of the high activity of the hybrids, they show a moderate loss in the DME production with TOS that denotes some kind of deactivation of the acidity function under reaction conditions.

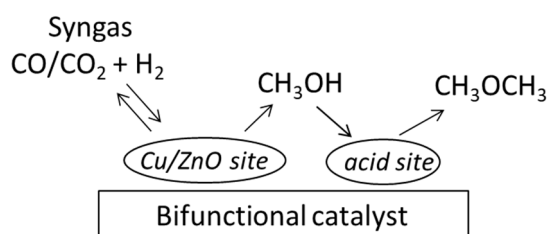
Keywords: DME; syngas; copper; zinc; heteropolyacids; titanium oxide

1. Introduction

The selective hydrogenation of CO/CO₂ into dimethyl ether (DME) is currently one of the most important topics in the research of alternative fuels because DME can be used as a direct and cleaner fuel alternative to conventional diesel [1]. In addition, DME is also an important chemical intermediate for the production of widely used chemicals, such as diethyl sulphate, methyl acetate or olefins [2]. DME is considered an ultra-clean transportation fuel because it has a high cetane number (around 60), low boiling point (−25 °C) and high oxygen content (35 wt %) which allow fast vaporization and higher combustion quality (smokeless operation and 90% less NO_x emissions) than other alternative CO₂-based fuels [2]. DME showed total compliance with the highly strict California ultra-low emission

vehicle (ULEV) regulations for medium-duty vehicles and it has the highest efficiency of all synthetic liquid fuels (e.g., F-T diesel, methanol) [3].

DME production is a well-established two-step industrial process: first catalytic hydrogenation of syngas into methanol ($\text{CO}/\text{CO}_2 + 3\text{H}_2 \rightarrow \text{CH}_3\text{OH} + \text{H}_2\text{O}$) and a subsequent catalytic dehydration of the methanol over acid catalysts to produce DME ($2\text{CH}_3\text{OH} \rightarrow \text{CH}_3\text{OCH}_3 + \text{H}_2\text{O}$). The main problem of this two-step DME synthesis derives from the strong thermodynamic limitation of the methanol synthesis step that leads to low gas conversion per pass (15–25%) and therefore high recirculation ratios and high capital and operating costs. To avoid this limitation, in the early 1990s researchers began to study the direct synthesis of DME in a process in which methanol synthesis step is coupled in situ with the dehydration step in a single reactor ($2\text{CO}/\text{CO}_2 + 6\text{H}_2 \rightarrow \text{CH}_3\text{OCH}_3 + 3\text{H}_2\text{O}$). The direct synthesis of DME allows increasing the level of conversion per step, up to 90%, which means significant savings in capital investment and production costs of DME. In fact, it is estimated that DME production costs in direct synthesis are reduced by 20–30% compared to the traditional two-step process. Direct DME synthesis requires highly efficient hybrid bifunctional catalytic systems which should combine a CO/CO_2 hydrogenation function for methanol synthesis and an acidic function for methanol dehydration (Scheme 1).



Scheme 1. Direct synthesis of dimethyl ether (DME) from syngas on bifunctional catalyst.

According to the mechanism operating in the direct synthesis of DME, the activity and efficiency of the hybrid bifunctional catalysts depend on: (i) the development of effective active sites for methanol synthesis, (ii) the control of the nature and strength of the acid sites (Brønsted/Lewis), (iii) the control of the balance between methanol synthesis sites and acid sites, and (iv) an adequate distance between the methanol synthesis sites and the acid dehydration sites [4]. The state-of-the-art in the development of the hybrids catalysts for the direct synthesis of DME are based on Cu-ZnO(Al) catalysts, as component for methanol synthesis, and zeolites (mainly HZSM-5) as acid component for methanol dehydration due to their hydrophobic nature and predominant Brønsted acid sites [5]. In the hybrid bifunctional catalysts, defects in the Cu particles, changes in the morphology of the Cu particles, dispersion, crystallite size and interaction of Zn atoms with the metallic Cu particles are important factors that define the activity for the methanol synthesis component [6–8] while the nature (Brønsted or Lewis), the acid strength (weak to medium) as well as the textural properties (mesoporosity) of the acid sites play fundamental roles for the methanol dehydration functionality [9,10]. Despite the great variety of synthesis methods (physically mixture, co-precipitation, sonochemical integrated, ...) and promoters or modifiers (MgO, ZnO, Na, Co, Fe, La, Ce, ...) explored so far for the preparation of Cu-ZnO(Al)-HZSM-5 hybrid catalysts, the catalytic activity of these hybrids decrease with time on stream owing to the deactivation by water, that produces copper oxidation or sintering [4], by strong interactions between the Cu-ZnO(Al) catalyst and the zeolite, that produces Cu migration [11] and by coke deposition [12]. Therefore, the effectiveness of Cu-ZnO(Al)-HZSM-5 catalysts is still limited and it is necessary considerable effort in catalysts development to improve its level of activity and durability.

Acid materials which are highly promising to avoid the inconveniences associated with the use of HZSM-5 zeolites are the heteropolyacids (HPAs). The HPAs exist in different structures and possess a very high Brønsted acidity, close to the super-acid region, and defined molecular structures. Therefore, they generally allow efficient dehydration of methanol under milder conditions than conventional

HZSM-5 acid catalysts, offering economic and environmental advantages [13]. The most studied HPAs for the methanol-to-DME process are those having the Keggin structure and the most acidic ones, namely $H_3PW_{12}O_{40}$ and $H_4SiW_{12}O_{40}$. Keggin HPAs consist of cubic crystals of heteropolyanions with formula $[XM_{12}O_{40}]^{n-}$ (X is the heteroatom (P^{5+} , Si^{4+}) and M is the so-called *addenda* atom, typically Mo^{6+} , W^{6+}) and stabilized by protons [14]. The HPAs are structured in three levels: (i) primary structure, corresponding to the heteropolyanion itself; (ii) secondary structure including the three-dimensional organization with H^+ and H_2O and, (iii) the tertiary structure including the arrangement of the particles responsible for the surface area of HPA. The location, number and strength of active acid sites for methanol dehydration in HPA are controlled by their structure (primary, secondary and tertiary) which is mainly determined by the water content in the HPA [15,16]. Up to 180 °C, six crystallization water molecules are in each Keggin unit forming a cubic structure in which $H_5O_2^+$ ions link four $[XM_{12}O_{40}]^{n-}$ anions [15]. The flexibility of the lattice of HPAs to absorb polar molecules as methanol and react in the solid bulk (pseudo-liquid behaviour) has as direct consequence the improvement in the activity in the dehydration of methanol over HPAs because the reaction takes place on both surface and bulk acid sites [17]. Therefore, water plays a main role in the acid activity of HPAs because it determines the strength and accessibility of the methanol to these acid sites and they could be altered by thermal treatments or by modification of the metal-oxygen clusters in the local structures of the Keggin units [16]. In addition, the HPAs have limited surface area (around 5–10 m²/g) and therefore to improve the availability to their inner protons, the dispersion of HPAs on neutral or acidic porous supports is often investigated (SiO_2 , ZrO_2 , Nb_2O_5 , TiO_2 , boron nitride,...) [18–22]. One of the most studied support in the methanol-to-DME reaction has been TiO_2 and the results have shown higher accessibility of supported HPA that means higher conversion of methanol per mass unit than unsupported counterparts [19]. However, remarkable differences in methanol dehydration were observed depending on the HPA loading and the interaction of HPA with the TiO_2 support because these interactions change the oxygen-metal bonds in the Keggin units modifying their acidity strength and accessibility [19].

Despite the considerable attention paid to the HPAs applied to methanol dehydration for production of DME, their use in hybrid bifunctional catalysts combined with Cu-ZnO(Al) catalysts for direct synthesis of DME from syngas has not yet been explored. The use of HPAs in hybrid catalysts poses new challenges to the heteropolyacids because they will be used under different reaction conditions ($T = 225\text{--}275$ °C, $P > 30$ bar) to that used in the dehydration of methanol ($T = 180\text{--}200$ °C, atmospheric pressure). In addition, the possible detrimental interaction of metallic copper with acid sites of HPAs, as previously observed in Cu-ZnO/ γ - Al_2O_3 [23] and Cu-ZnO(Al)/HZSM-5 hybrids [24] could produce partial deactivation of both functionalities. Two main causes for the detrimental interaction of metallic copper with acid sites in hybrid bifunctional catalysts has been reported: (i) Cu sintering [4] or (ii) copper and zinc ion exchange with protons of zeolite [24].

In this scenario, this work was undertaken with the aim to study for the first time the performance of bifunctional hybrids based on phosphotungstic acid ($H_3PW_{12}O_{40}$) supported on TiO_2 combined with Cu-ZnO(Al) catalyst in the direct synthesis of DME from syngas. Taking into account that local structure of Keggin units depends on the interaction established between the Keggin units with the TiO_2 support, in this work we studied specifically the effect of the heteropolyacid loading on the dispersion and acid characteristics of HPAs and its relevance on the hybridization with CZA catalyst applied for the direct synthesis of DME from syngas. Individual and hybrid catalysts were well-characterized (XRD, Raman, DRIFTS, H_2 -TPR, N_2O chemisorption and NH_3 -TPD) in order to establish the relationships between the properties of individual functionalities (methanol synthesis and methanol dehydration) and their role in the activity of the hybrids in the direct synthesis of DME from syngas.

2. Results and Discussion

2.1. Structure and Acidity of xHPW/Ti Acid Catalysts

The diffraction profiles of the xHPW/Ti acid catalysts are collected in Figure 1. All catalysts show diffraction peaks (25.3, 36.9, 37.7 and 38.5; 27.4 and 36.0°) characteristic of the anatase (Joint Committee on Powder Diffraction Standards, JCPDS 21-1272) and rutile (Joint Committee on Powder Diffraction Standards, JCPDS 21-1276) phases respectively of the TiO₂ support. In addition to the diffraction lines of the TiO₂ support, the samples also show diffraction lines at 10.2, 14.5, 17.8, 20.6, 23.1, 25.3, 27.4, 29.3, 31.2, 32.9 and 34.5° associated with crystalline cubic H₃PW₁₂O₄₀·6H₂O species [15]. As expected, the intensity of the diffraction peaks corresponding to these crystalline structures increases upon increasing the heteropolyacid loading (Table 1). However the increase in intensity was not linear with the HPW loading with a marked increase in the crystallinity and domain size of HPW when its content exceeds 1.7 theoretical monolayers (Table 1). In the case of the 1.7HPW/Ti sample, it is also observed a slight peak at 26.2° with some shoulders at 10.6, 15.1 and 21.4° related to small crystals of cubic H₃PW₁₂O₄₀·3H₂O [25]. The loss of water in H₃PW₁₂O₄₀·6H₂O produces a contraction in its structure as is evidenced through the shift of diffraction peaks at higher angles [25,26]. According to the literature, dispersed H₃PW₁₂O₄₀·6H₂O could be dehydrated with formation of H₃PW₁₂O₄₀·3H₂O at lower temperature than that observed on the bulk (180 °C) [25] because the interaction of HPA entities with the support weakens and facilitates the water loss from the cubic Keggin structures [27].

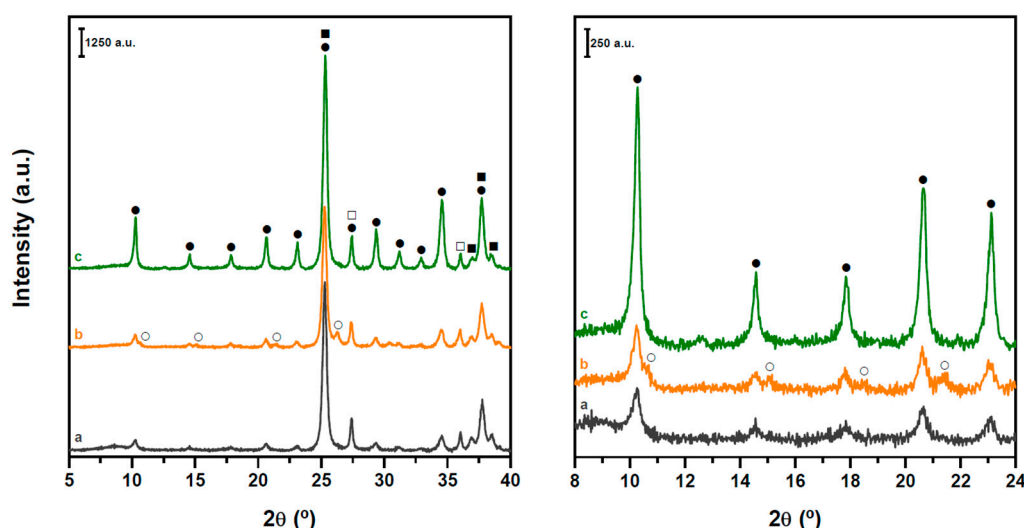


Figure 1. XRD patterns of xHPW/Ti acid catalysts: 1.4HPW/Ti (a), 1.7HPW/Ti (b) and 2.7HPW/Ti (c) (anatase (■), rutile (□), H₃PW₁₂O₄₀·6H₂O (●) and H₃PW₁₂O₄₀·3H₂O (○)).

Table 1. Relative intensity and particle size of HPW·6H₂O (from XRD), acid/neutral water (from DRIFTS) and relative intensity of HPW (from Raman) of xHPW/Ti acid catalysts.

	HPW·6H ₂ O Relative XRD Intensity (a.u.)	HPW·6H ₂ O dp (nm)	Acid/Neutral Water Ratio (1700/1620 cm ⁻¹)	HPW/TiO ₂ Relative Raman Intensity (990/650 cm ⁻¹)
1.4HPW/Ti	1.0	20.5	0.423	0.371
1.7HPW/Ti	1.47	17.6	0.403	0.365
2.7HPW/Ti	4.6	30.6	0.784	0.536

Figure 2 shows DRIFT spectra of the xHPW/Ti acid catalysts. In the region of the vibration modes corresponding to the metal-oxygen, the titania support presents an asymmetric contribution centered on 778 cm⁻¹ (Ti–O–Ti, stretching). The spectra of xHPW/Ti acid catalysts show contributions characteristic of HPW: at 1080 cm⁻¹, corresponding to P–O_a asymmetrical stretching; at 984 cm⁻¹,

associated to $W-O_d$ stretching terminal oxygen; at 888 cm^{-1} , ascribed to $W-O_b-W$ corner-shared bridged bond and, finally a broad band at 816 cm^{-1} , corresponding to $W-O_c-W$ edge-shared bridged bond [28–30]. As the HPW load increases, an increase in the relative intensity of the HPW signals is observed in metal-oxygen bonds region ($1200\text{--}600\text{ cm}^{-1}$) with respect to the vibration modes of the titania support. There is no significant displacement or widening of the HPW signals in the xHPW/Ti acid catalysts which indicates that the Keggin structure of HPW has not been significantly distorted after supporting on TiO_2 .

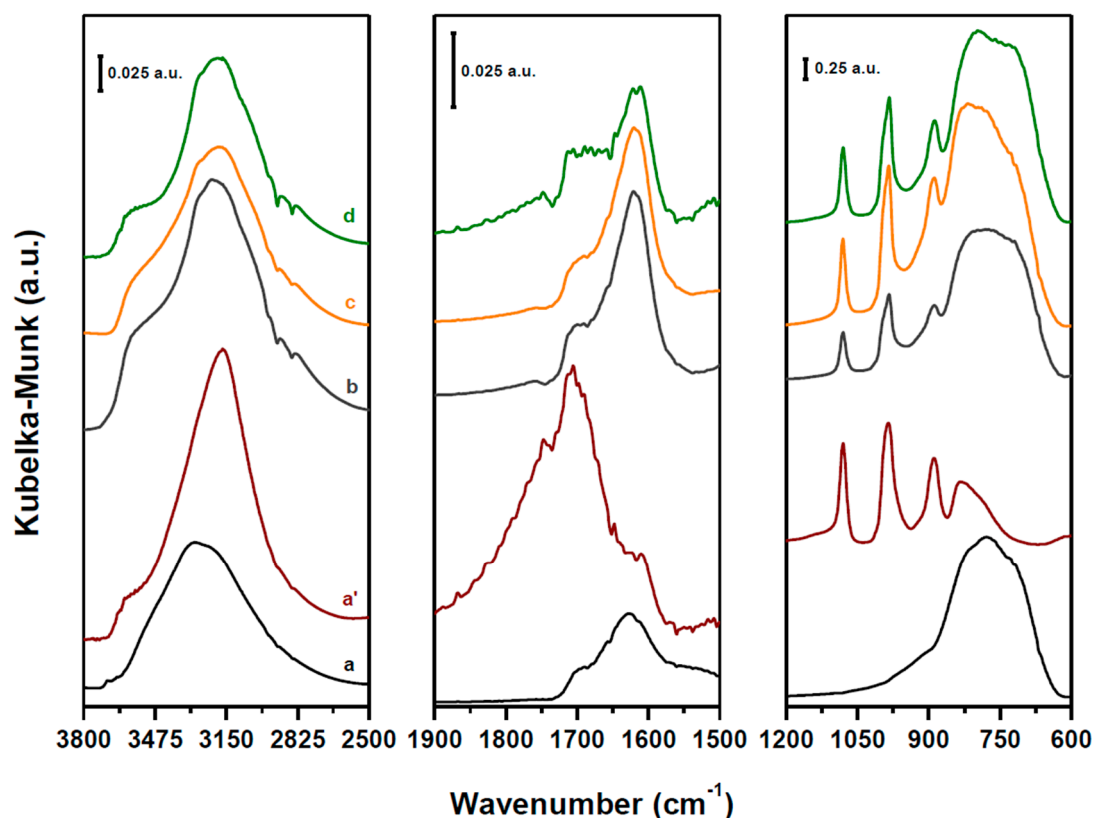


Figure 2. DRIFT spectra at room temperature of TiO_2 support (a), bulk HPW (a') and xHPW/Ti acid catalysts: 1.4HPW/Ti (b), 1.7HPW/Ti (c) and 2.7HPW/Ti (d).

In the region $3800\text{--}2500\text{ cm}^{-1}$, the titania support (Figure 2a) presents a broad band around 3332 cm^{-1} corresponding to physisorbed water molecules and contributions at 3528 and 3638 cm^{-1} ascribed to isolated hydroxyl groups on TiO_2 and dissociatively adsorbed water on TiO_2 respectively [31]. The physisorbed water on TiO_2 was corroborated by the band of the OH bending at 1636 cm^{-1} [32]. The xHPW/Ti acid catalysts also show in the $3800\text{--}2500\text{ cm}^{-1}$ region a band centered around 3300 cm^{-1} which includes physisorbed water and protonated water in the dioxonium ions ($H_2O-H^+-H_2O$) [33] and a separated band at 3638 cm^{-1} due to hydroxyl groups on TiO_2 or dissociatively adsorbed water on TiO_2 . The relative intensity of this latter band decreases in parallel with the HPW loading which is indicative of the decrease of hydroxyl groups of TiO_2 covered by HPW units. In the water bending region, the xHPW/Ti acid catalysts show two bands at 1712 and 1620 cm^{-1} , attributed to the bending O-H vibration of dioxonium $H_2O_5^+$ and neutral water respectively [34]. The relative intensity of the acid/neutral water ratio in the xHPW/Ti acid catalysts, calculated from the relative area of the bands at 1712 and 1620 cm^{-1} , is not proportional to the HPW loading (Table 1). The samples with 1.4 and 1.7 monolayers show a similar ratio, while the sample with 2.7 monolayers shows a marked increase in the relative amount of acid water.

The evolution of xHPW/Ti samples upon heating under He flow (25–150–200 and 250 °C) was followed by DRIFT and the corresponding spectra were collected in Figure 3. The bands corresponding to neutral water (3638, 3300 and 1620 cm^{-1}) and acidic water (3300 and 1710 cm^{-1}) decreases as the temperature increase and disappear at 250 °C while the bands corresponding to metal-oxygen bonds of the Keggin structure do not suffer modification. This later fact contrast with the reported splitting of the band at 984 cm^{-1} ($\text{W}=\text{O}_d$) for dehydrated bulk heteropolyacids [15,35]. As the splitting is related with the $\text{W}=\text{O}$ groups which the oxygen participates/non participate in the formation of hydrogen bonds with neighboring KU, the absence of splitting in dehydrated xHPW/Ti may indicate low participation of the oxygen in the formation of hydrogen bonds between KU units when they are supported. The temperature at which the acidic water disappears on the xHPW/Ti acid catalysts is higher than that observed on bulk HPW (results not shown here) in which the acid water was removed at 150 °C. In addition, the removal of the acidic water on the xHPW/Ti samples depends on its HPW loading being lower when the HPW concentration increases. Therefore, it seems to indicate that supported HPW at low loading on TiO_2 stabilizes its protonated water molecules.

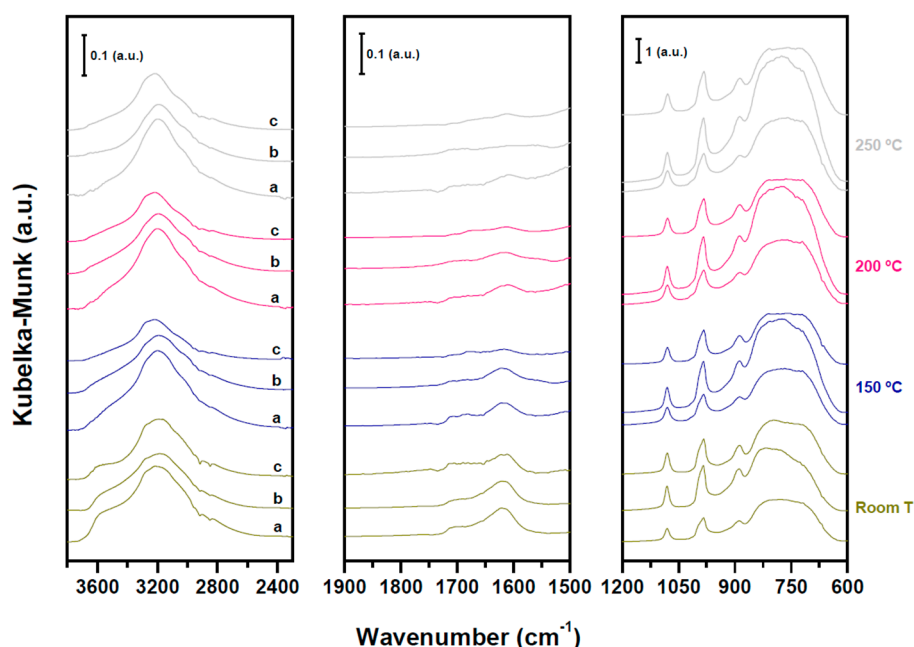


Figure 3. DRIFT spectra of xHPW/Ti acid catalysts upon heating under He flow (25–150–200 and 250 °C): 1.4HPW/Ti (a), 1.7HPW/Ti (b) and 2.7HPW/Ti (c).

The structure of the xHPW/Ti acid catalysts was also studied by Raman spectroscopy as shown in Figure 4. The Raman spectra of all xHPW/Ti samples show bands at 638, 517, 397 cm^{-1} and a small shoulder at 450 cm^{-1} characteristic of the anatase and rutile phases of the TiO_2 support respectively [36,37]. The samples also show Raman bands at 216, 236–239, 990 cm^{-1} and 1009 cm^{-1} assigned to $\text{W}-\text{O}-\text{W}$ bending, $\text{W}=\text{O}_d$ symmetric stretch and $\text{W}=\text{O}_d$ asymmetric stretch respectively [38–40], which demonstrate the existence of Keggin structures of HPW on the TiO_2 support. The Raman HPW signals become more intense as the concentration of HPW in the catalysts increases (Table 1) which confirms, in agreement with the previous XRD results, the higher development of crystalline structures of HPW in the catalysts with higher heteropolyacid loading. However some widening and shift of the HPW Raman bands was observed in the sample with the lower HPW loading (1.4HPW/Ti) which suggests greater interaction between the oxygen atoms of the HPW and the hydroxyl groups of the support at low heteropolyacid loading [41–43].

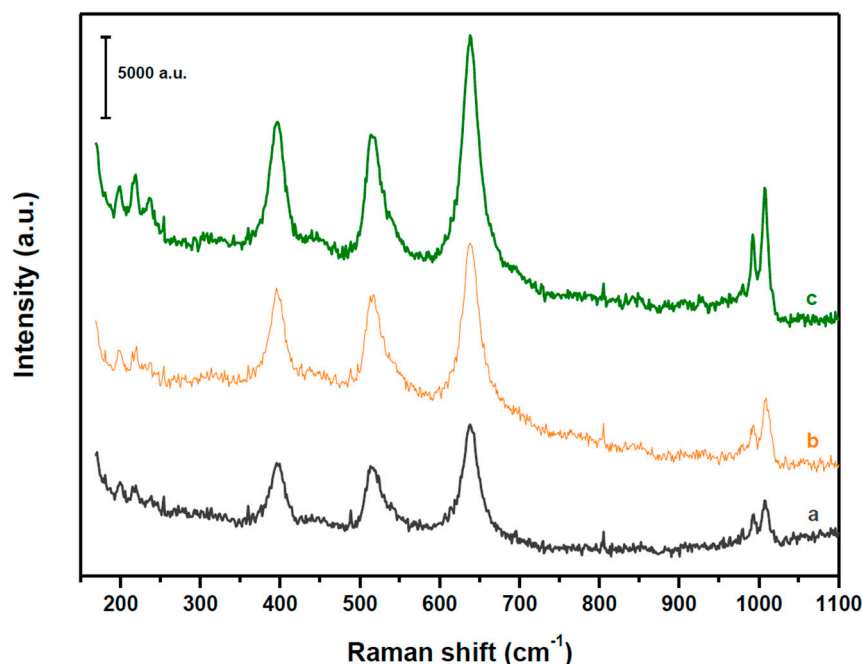


Figure 4. Raman spectra of HPW/Ti acid catalysts: 1.4HPW/Ti (a), 1.7HPW/Ti (b) and 2.7HPW/Ti (c).

The acidity of the xHPW/Ti samples was determined by temperature-programmed desorption of ammonia whose profiles are depicted in Figure 5. The TPD profiles show two main regions: low-medium temperature (LT-MT, ~125–400 °C) and high temperature region (HT ~550 °C). The peak at LT-MT corresponds to weak-medium acid sites associated with Lewis sites (un-coordinated Ti^{4+} ions) of the TiO_2 support [44] while the peak at high temperature corresponds to the decomposition of $(\text{NH}_4)_3\text{PW}_{12}\text{O}_{40}$ formed by reaction of the strong acid sites of HPW with NH_3 [45,46]. Integration of the weak-medium acid sites (LT-MT region, Table 2) shows no clear relationship with the HPW loading, presenting the sample with 1.7 monolayers the higher concentration of weak-medium sites related with the TiO_2 support. On the contrary, the intensity and desorption temperature of the strong acid sites related with the HPW entities (HT, Table 2) increases as the HPW load in the catalyst increases. This shift could be consequence of the higher dispersion or interactions of the HPW with the support at lower loading that affect the decomposition of the ammonium salts formed by reaction of NH_3 with the supported HPW entities [22]. Assuming that the unsupported bulk HPW has three acidic protons for each Keggin unit (KU), the number of acidic protons in the xHPW/Ti catalysts has been estimated based on the relative area ratio of the HT peaks (Table 2). Based on this calculation, the number of acidic protons per KU on the xHPW/Ti varies with the HPW loading increasing from 1.26 H^+/KU in the 1.4HPW/Ti sample up to 2.37 H^+/KU , close to bulk HPW, in the 2.7HPW/Ti sample. This fact is line with previous works in the literature [42,47] that has shown the loss of acidic protons of HPW by the formation of strong H-bonds with available OH groups on the supports.

Table 2. Quantitative data from TPD- NH_3 profiles of xHPW/Ti acid catalysts.

	Area (LT-MT)	Area (HT)	H^+/KU
1.4HPW/Ti	93.25	108.12	1.26
1.7HPW/Ti	177.31	132.65	1.55
2.7HPW/Ti	108.54	202.72	2.37
HPW	-	215.15	3.0

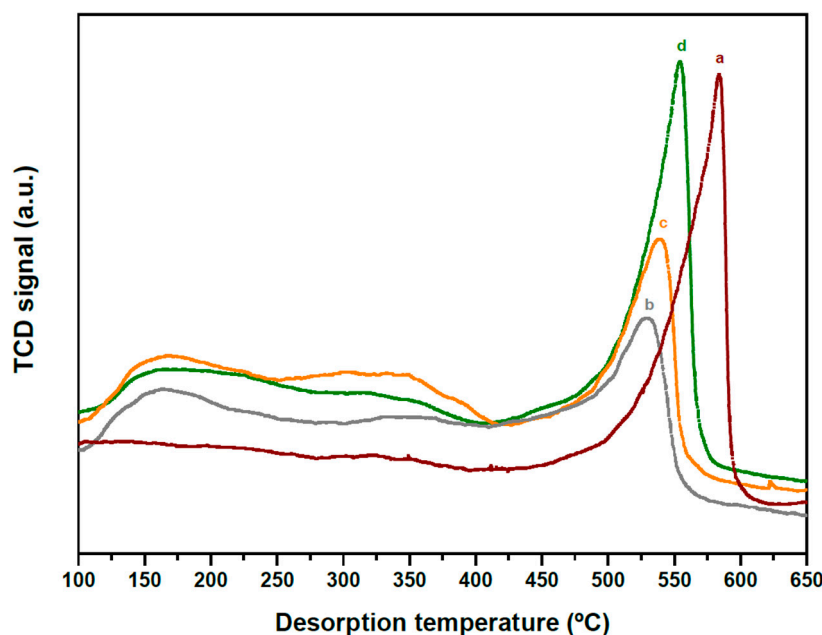


Figure 5. TPD-NH₃ profiles of bulk HPW (a) and xHPW/Ti acid catalysts: 1.4HPW/Ti (b), 1.7HPW/Ti (c) and 2.7HPW/Ti (d).

2.2. Structure and Acidity of CZA-xHPW/Ti Bifunctional Hybrid Catalysts

The morphological characteristics of the CZA-HPW/Ti hybrid catalysts in comparison with the CuO/ZnO(Al) catalyst (CZA) were studied by SEM (Figure 6). The SEM image of the bare CZA catalyst shows the typical irregular agglomerates formed by particles of different size and morphology observed in this kind of catalysts [6]. The CZA-HPW/Ti hybrid catalysts shows similar morphology maintaining the morphological characteristics of the agglomerates previously observed in the bare CZA. It is observed that the small HPW/Ti particles (arrows in Figure 6) are in surface contact with the CZA agglomerates without achieving a homogenous distribution and covering of the CZA particles.

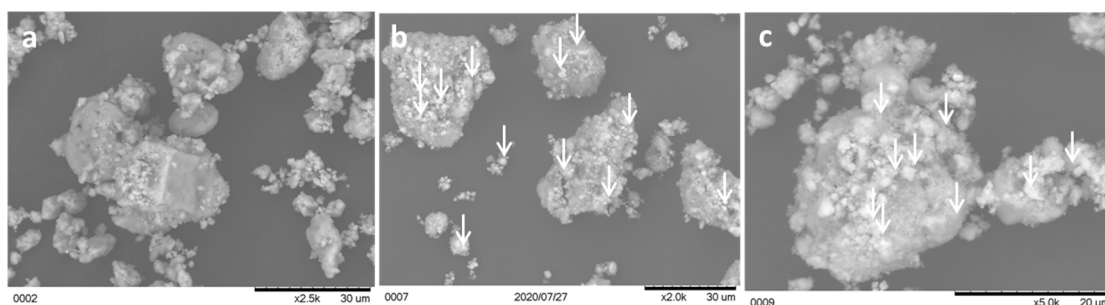


Figure 6. SEM images showing the morphology of calcined CZA-xHPW/TiO₂ hybrid catalysts: pristine CZA (a), CZA-1.4HPW/Ti (b), CZA-2.7HPW/Ti (c) (arrows indicate HPW/Ti particles).

Figure 7 shows the XRD patterns of the CZA-HPW/Ti hybrid catalysts in comparison with the CuO/ZnO(Al) catalyst (CZA) as reference. The pristine CZA shows broad diffraction peaks corresponding to CuO (JCPDS 1-117) and small peaks of ZnO (JCPDS 43-002) with crystallite size around 4.5 and 5 nm respectively (Table 3). The diffractograms of the CZA-HPW/Ti hybrid catalysts show the diffraction peaks corresponding to CuO and ZnO previously observed in the pristine CZA indicating no noticeable changes in their crystalline size after hybridization. The hybrid catalysts also show the diffraction peaks at 25.2, 37.8, 47.9 and 27.4° assigned to the anatase and rutile phases of TiO₂ as well as the main diffraction peaks assigned to crystalline HPW structures. In the case of the

HPW structures, their diffraction peaks are shifted to higher angles which indicates lattice contraction associated to dehydration with formation of the cubic HPW·3H₂O phase after hybridization [25]. The dehydration is complete for the hybrids with 1.4 and 1.7 HPW monolayers while in the sample with 2.7 monolayers remains a slight contribution of the hydrated HPW·6H₂O. The intensity and size of the crystalline HPW structures on the hybrids (Table 3) increase with the HPW loading similarly to that observed in the case of the non-hybridized xHPW/Ti acid catalysts. The dehydration on HPW structures after hybridization with CZA could be related with the intimate contact between them that allows the migration of water from HPW to CZA taking into account the diffusivity of water on TiO₂ [48] and the capacity of CZA to be rehydrated by the carbonates retained in its structure [49].

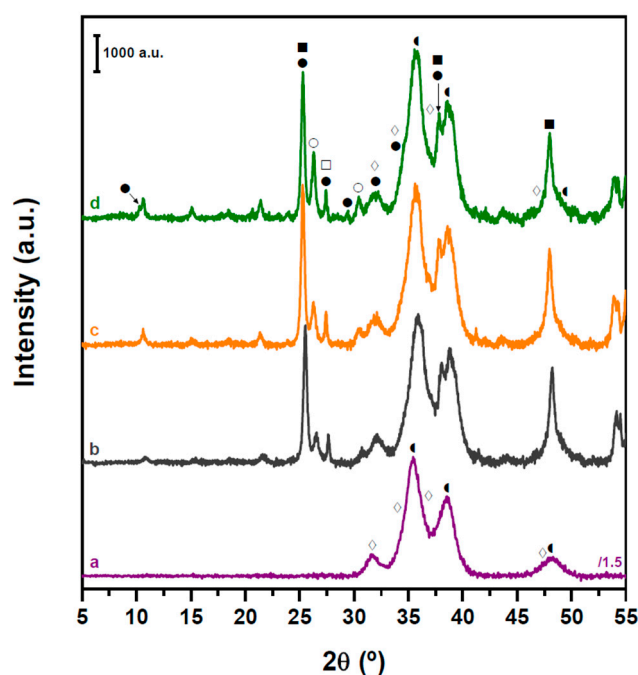


Figure 7. XRD patterns of calcined CZA-xHPW/TiO₂ hybrid catalysts: pristine CZA (a), CZA-1.4HPW/Ti (b), CZA-1.7HPW/Ti (c), and CZA-2.7HPW/Ti (d) (anatase (■), Rutile (□), H₃PW₁₂O₄₀·6H₂O (●), H₃PW₁₂O₄₀·3H₂O (○), ZnO (◇) and CuO (▲)).

Table 3. Crystallite size (nm from XRD) of Cu, CuO and ZnO in CZA and CZA-xHPW/Ti hybrids catalysts in calcined and reduced state and specific surface area (N₂O chemisorption) of copper in reduced hybrid catalysts.

	Calcined			Reduced		
	CuO	ZnO	HPA·3H ₂ O	Cu	ZnO	Cu Surface Area
	dp (nm)	dp (nm)	dp (nm)	dp (nm)	dp (nm)	(m ² /g _{cat})
CZA-1.4HPW/Ti	4.5	5.1	11.4	5.1	6.3	28.6
CZA-1.7HPW/Ti	4.4	5.3	4.4	5.4	6.1	35.5
CZA-2.7HPW/Ti	4.8	5.3	4.8	5.7	6.5	39.1
CZA	4.5	4.9	-	5.1	6.7	43.4

The reducibility of the CZA-HPW/Ti hybrid catalysts was studied by temperature-programmed reduction (Figure 8). The pristine CZA catalyst exhibits a small broad peak around 155 °C followed by a second main reduction peak around 180 °C. The first peak is ascribed to the reduction of highly dispersed CuO in undecomposed carbonate species while the second main peak is related with the reduction of CuO nanoparticles interacting with ZnO [50]. The reduction profiles of the CZA-HPW/Ti

hybrid catalysts are not significantly altered respect to the pristine CZA catalyst, with the main reduction peak around 180 °C attributed, as indicated above, to the reduction of CuO nanoparticles in contact with ZnO. However, it is observed as the amount of HPW in the hybrid increases a decrease in the reduction peak at low temperature and a widening of the main reduction peak with separation of two contributions that indicates heterogeneous reducibility of CuO and their contacts with ZnO. The decrease of the reduction peak at low temperature in the hybrids corresponding to the highly dispersed CuO in undecomposed carbonate species could be related with the above commented migration of water from HPW to CZA that could rehydrate these carbonates altering its reducibility [49]. The widening in the main reduction peak is probably derived from the absence of the small peak at 155 °C that is known that facilitates the subsequent reduction of the CuO species [51].

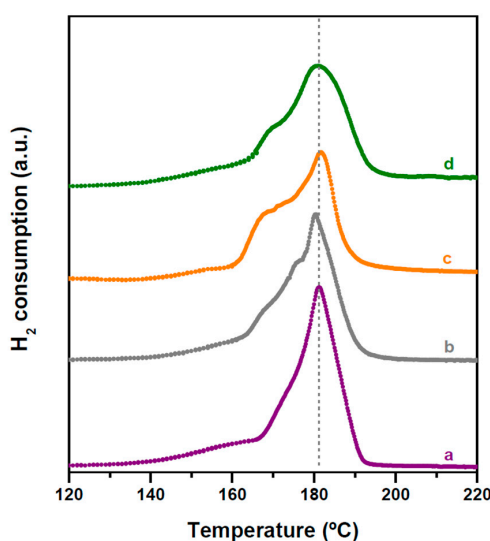


Figure 8. Temperature-programmed reduction (TPR) profiles of pristine CZA (a) and CZA-xHPW/Ti hybrid catalysts: CZA-1.4HPW/Ti (b), CZA-1.7HPW/Ti (c) and CZA-2.7HPW/Ti (d).

XRD profiles of reduced CZA-HPW/Ti hybrid catalysts are depicted in Figure 9. All reduced hybrid catalysts show diffraction peaks corresponding to reflections of metallic Cu (43.0 and 50.2° JCPDS 001-1241) and ZnO phases (31.7, 34.8, 36.3 and 47.0°, JCPDS 075-0576). The size of the crystalline domains of copper in reduced CZA-HPW/Ti hybrid catalysts was similar to that of the pristine reduced CZA but increases slightly with the HPW loading in the hybrid (Table 3). The diffraction peaks corresponding to the HPW·3H₂O cubic phase detected on the calcined CZA-xHPW/Ti hybrid catalysts (Figure 6) appears now as small peaks in the reduced catalysts (Figure 9) which means the almost total dehydration and amorphization of HPW, which increases with the HPW loading, [25] after the reduction treatment.

The Cu surface area, the contacts of Cu nanoparticles with reduced zinc species or defects in copper particles in the CZA-xHPW/Ti hybrid catalysts have been evaluated by N₂O chemisorption [52] and the results were collected in Table 3. The pristine CZA catalyst exhibits very high specific Cu surface area (43.4 m²/g) in line with the best catalysts published for methanol synthesis. The Cu surface area of the reduced hybrid catalysts decreases respect to the pristine CZA, with the decrease being less significant as the HPW load in the hybrid increases (CZA-1.4HPW/Ti < CZA-1.7HPW/Ti < CZA-2.7HPW/Ti, Table 3). Since XRD and TPR data did not show appreciable changes in the average Cu⁰ particle size or reducibility for the hybrid catalysts with respect to the CZA catalyst, the observed variations in the Cu surface area probably reflect: (i) physical blockage of Cu sites by the xHPW/Ti particles [12] or, (ii) modifications in the Cu-ZnO interactions associated with the migration of Cu²⁺ or Zn²⁺ species from the CZA to the acid catalyst which has been identified as main cause of deactivation in of the hybrids formed by Cu-ZnO(Al) and acid catalysts [53–55].

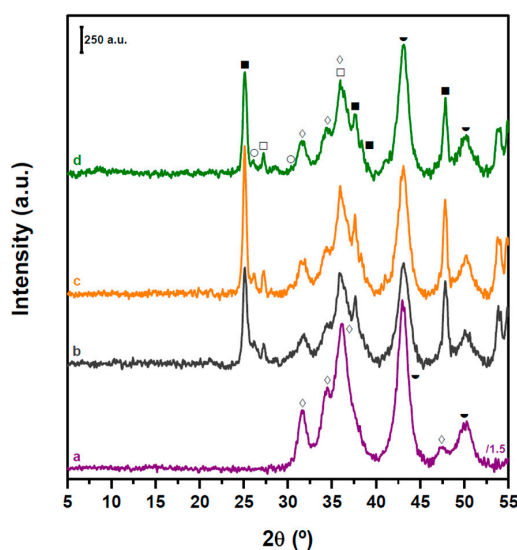


Figure 9. XRD patterns of reduced pristine CZA (a) and reduced CZA-xHPW/TiO₂ hybrid catalysts: CZA-1.4HPW/Ti-r (b), CZA-1.7HPW/Ti-r (c) and CZA-2.7HPW/Ti-r (d) (anatase (■), Rutile (□), H₃PW₁₂O₄₀·3H₂O (○), ZnO (◇) and Cu⁰ (▼)).

The acid properties of reduced 1.4 and 2.7 CZA-HPW/Ti hybrids were evaluated by NH₃-TPD and the results were depicted in Figure 10. Significant differences have been found between the acid properties of the reduced CZA-xHPW/Ti hybrids with respect to the xHPW/Ti acid catalysts before hybridization (Figure 5). The reduced CZA-xHPW/Ti hybrids show similar desorption profile regardless of the HPW loading with desorption peaks between 200 and 400 °C that corresponds to acid sites of weak or medium strength. According to literature studies, the acid sites of weak and/or moderate strength are the most desirable for DME selectivity since the strong Brönsted acid sites favour the conversion of DME to hydrocarbons [11,56]. The medium-weak acid sites observed in the reduced hybrids contrast with the very strong acid sites detected on the xHPW/Ti acid catalysts before hybridization (550–600 °C, Figure 5). This finding indicates that hybridization with CZA catalysts gives rise to a decrease in the acid strength of the HPW with the disappearance of the strong acidic sites typical of pristine HPW units. A similar behaviour, suppression of Brönsted acidity of zeolites after hybridization with Cu-ZnO catalysts, was already observed in the literature [24,57] and attributed to the exchange of protons with Cu²⁺ and/or Zn²⁺ cations from Cu-ZnO occurring during the hybrid preparation. In line with this, the partial exchange of protons of heteropolyacids with metal cations (Cu^{II}, Al^{III}, Sn^{IV}, Fe^{III}, Cr^{III}, Zr^{IV}, Zn^{II}, ...) has been reported producing Lewis sites with the concomitant reduction in the amount of Brönsted sites [58,59]. To support the inter-cationic exchange between Cu²⁺ and/or Zn²⁺ and protons in CZA-xHPW/Ti hybrids, they are characterized by DRIFTS (Figure 11) because the structural modes of the KU, between 1150 and 700 cm⁻¹, are sensitive to changes in its composition [35]. The DRIFTS spectra of CZA-xHPW/Ti hybrids show the characteristic bands of the Keggin structure at around 1080, 983, 886 and 800 cm⁻¹ already identified in non-hybridized dehydrated xHPW/Ti counterparts (Figure 3). However, the hybrids show slight displacements and shoulders at 1053 and 952 cm⁻¹ that may indicate certain alterations in the structure derived to the change in the composition of the compensating cations, able to interact with terminal and/or bridging oxygens of the Keggin units [59,60]. This result is consistent with the exchange of H⁺ in HPW by Cu²⁺/Zn²⁺ and it may be the cause of the reduction in the amount of Brönsted acidity of xHPW/Ti observed by NH₃-TPD after the hybridization with CZA. The migration of Cu²⁺/Zn²⁺ species from CZA to xHPW/Ti could proceed through the *contact-induced ion exchange* mechanism described in literature to explain the exchange of cationic species between zeolites by simple physical contact and mediated by water adsorbed on the pores [61,62].

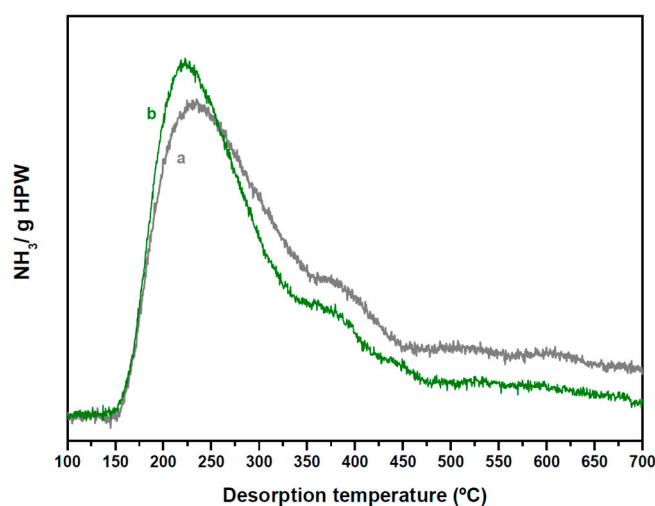


Figure 10. TPD-NH₃ profiles of reduced CZA-xHPW/TiO₂ hybrid catalysts: CZA-1.4HPW/Ti (a) and CZA-2.7HPW/Ti (b).

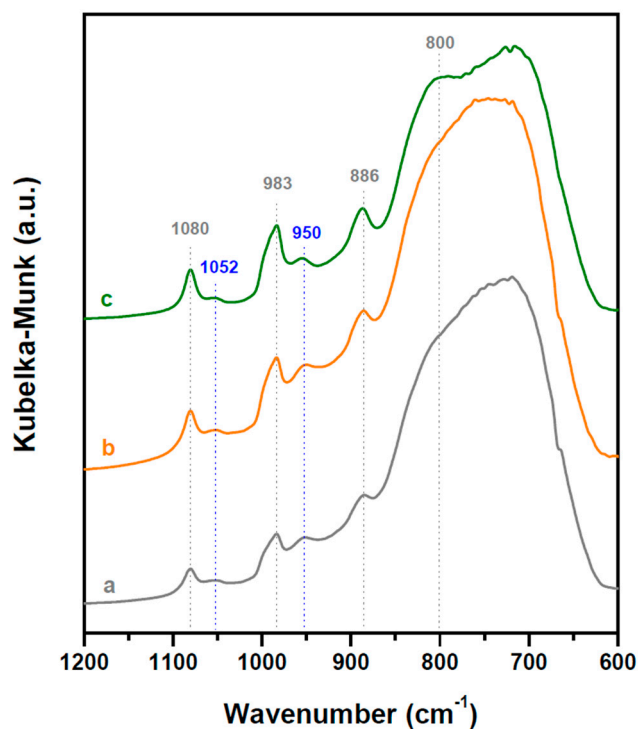


Figure 11. DRIFT spectra of CZA-xHPW/Ti hybrid catalysts: CZA-1.4HPW/Ti (a), CZA-1.7HPW/Ti (b) and CZA-2.7HPW/Ti (c).

2.3. Activity in Direct Synthesis of DME from Syngas

The activity of the CZA-HPW/Ti hybrid catalysts were evaluated for the direct DME synthesis from syngas (30 bar and 250 °C) and the activity data were collected in Table 4 and Figure 12. Activity data also includes the results for methanol synthesis on the CZA catalyst and the DME synthesis on the CZA-HZSM-5 hybrid reference representative of the most widely applied catalysts for direct synthesis of DME.

Table 4. Initial catalytic activity data (CO conversion, selectivity and DME time yield) and deactivation (decay in $\mu\text{mol}_{\text{DME}}/\text{min g}_{\text{cat}}$) in direct DME synthesis from syngas over reduced CZA-xHPW/Ti hybrid catalysts (Data for methanol synthesis on CZA and DME synthesis on CZA-HZSM-5 catalysts were included as references).

	CO Conversion (%)	Selectivity (%)		DME Time Yield		Deactivation Rate DME ($\mu\text{mol}/\text{min g}_{\text{cat}}$)
		Methanol	DME	CO ₂	($\mu\text{mol}/\text{min g}_{\text{cat}}$)	
CZA	17.6	98.9	-	1.1	967.3 *	0.22 *
HZSM-5-CZA	11.4	6.2	55.7	38.1	229.4	0.24
CZA-1.4HPW/Ti	14.5	97.4	2.5	0.1	12.3	0.06
CZA-1.7HPW/Ti	10.0	12.6	51.3	36.1	201.9	0.20
CZA-2.7HPW/Ti	11.0	6.4	53.0	40.6	243.0	0.14

* Methanol time yield and deactivation rate ($\mu\text{mol}/\text{min g}_{\text{cat}}$).

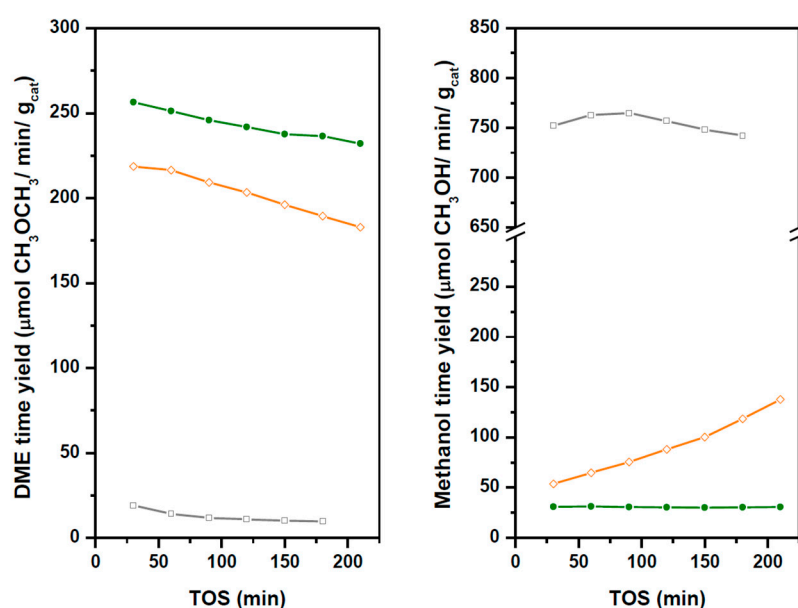


Figure 12. Methanol and DME time yield ($\mu\text{mol}/\text{min}/\text{g}$ catalyst) from syngas over CZA-1.4HPW/Ti (\square), CZA-1.7HPW/Ti (\diamond) and CZA-2.7HPW/Ti (\bullet).

The methanol activity on the CZA catalyst is very high ($967.3 \mu\text{mol}$, $\text{CH}_3\text{OH}/\text{min g}_{\text{cat}}$, Table 4) and comparable with the best data published in the literature [63]. As expected, the catalytic behaviour of the CZA-xHPW/Ti hybrid catalysts depend on their HPW loading. All CZA-xHPW/Ti hybrids only show methanol and DME as products without formation of hydrocarbons. The absence of hydrocarbons, from DME dehydration, could be justified because the acid sites present on the hybrids were of weak or medium strength (Figure 5) and because the formation of hydrocarbons requires higher contact-time than that used in our catalyst test [64]. The overall methanol and DME yield on CZA-HPW/Ti hybrids were in all cases lower than the methanol yield achieved on the CZA reference. This effect was also observed in other works in the literature but without discussing its causes [12,65]. Considering that overall DME production is controlled by the methanol synthesis step, the observed decrease in the overall yield on CZA-xHPW/Ti hybrids can be derived from detrimental effects on the CZA catalyst after hybridization. It is well established that the methanol synthesis activity on copper catalysts is directly related with its Cu surface area (reduced zinc species in contact with copper and/or defects in copper particles induced by their contact with Zn) [66]. According to the characterization of the CZA-xHPW/Ti hybrid catalysts, the Cu surface area in the hybrid catalysts, evaluated by N_2O chemisorption, shows a reduction in the hybrid catalysts respect to the pristine CZA (Table 3) and this fact may be the cause of the observed reduction in the overall yield on CZA-xHPW/Ti hybrid

catalysts respect the pristine CZA. However the sequence in the copper surface area in the hybrids (CZA-1.4HPW/Ti < CZA-1.7HPW/Ti < CZA-2.7HPW/Ti, Table 3) does not fit with the overall yield loss on the hybrids, presenting the sample with the smallest Cu surface area (CZA-1.4HPW/Ti) the highest overall yield in the hybrid series. Taking into account the parallelism between the DME production and the overall yield loss on the hybrids, a second cause to explain the overall yield loss may be related with detrimental interactions between CZA and the excess of water from DME production because the kinetics of the methanol formation is very sensitive to the water content [67]. In fact it is observed an increase in the CO₂ selectivity associated to the WGS reaction whose contribution increases with increasing water concentration. In addition to the inhibitory effect of the water on the methanol synthesis kinetics, water can also promote the sintering of copper particles [68]. However, the average copper particle size in used CZA-xHPW/Ti hybrids (determined by XRD Figure 13, Table 5) compared with the bare CZA demonstrated that excess of water from higher production of DME does not significantly affect the particle size as the Cu growth (8–13%) was similar in all used hybrids.

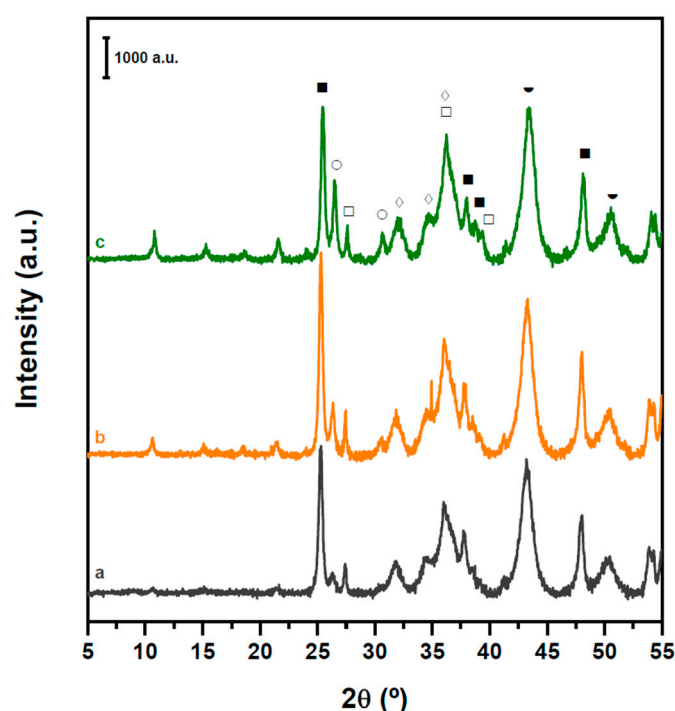


Figure 13. XRD patterns of used CZA-HPW/TiO₂ hybrid catalysts: CZA-1.4HPW/Ti-u (a), CZA-1.7HPW/Ti-u (b) and CZA-2.7HPW/Ti-u (c) (anatase (■), Rutile (□), H₃PW₁₂O₄₀·3H₂O (○), ZnO (◇) and Cu⁰ (▼)).

Table 5. Crystallite size (nm from XRD) of Cu and ZnO in CZA and CZA-xHPW/Ti hybrids catalysts in used state.

	Cu	ZnO
	dp (nm)	dp (nm)
CZA-1.4HPW/Ti	5.1	6.3
CZA-1.7HPW/Ti	5.4	6.1
CZA-2.7HPW/Ti	5.7	6.5
CZA	5.1	6.7

The relationship between the rate of the DME production and the acid strength of the catalysts is well documented in heteropoly acid catalysts [21]. The differences in acidity observed on xHPW/Ti catalysts (Figure 5, Table 2) disappear after hybridization, showing all the CZA-xHPW/Ti hybrids

similar acid sites of weak or medium strength (Figure 10). Therefore similar rate of DME production per acid site can be expected on the hybrids and the observed differences in the DME productivity on the hybrids (Table 4) would be due to the different concentration of acid sites according to its different HPW content. However it is observed that there is not linearity between the HPW content in hybrids and the production of DME (Figure 12). The lowest loaded hybrid catalyst (CZA-1.4HPW/Ti) was ineffective, with low DME selectivity (2.5%) while as the HPW loading in hybrids is increased the selectivity towards DME increases, reaching a maximum selectivity for DME (53.0%) for the highest HPW loaded hybrid catalyst (CZA-2.7HPW/Ti). The DME production over the most active CZA-2.7HPW/Ti hybrid catalyst ($260 \mu\text{mol}/\text{min g}_{\text{cat}}$) is significantly higher than that achieved on the CZA-HZSM-5 hybrid reference ($229 \mu\text{mol}/\text{min g}_{\text{cat}}$) representative of the most widely applied catalysts for direct synthesis of DME. The low effectivity for DME production of the CZA-1.4HPW/Ti sample could be related with the fact that the dehydration of methanol to DME improves in the pseudo-liquid behaviour of the HPW for which it is necessary to develop three-dimensional crystalline structures [69] and as can be seen in Figure 13 they are not formed at this HPW loading. On the contrary, three-dimensional HPW structures are clearly observed in the samples 1.7 and 2.7 CZA-xHPW/Ti [70] in which the pseudo-liquid behaviour could occur improving the methanol access to the acid sites and thus justifying the remarkable increase in DME production observed for these samples. The incomplete conversion of methanol to DME observed on the 1.7CZA-xHPW/Ti hybrid (Figure 12) means that the methanol dehydration reaction is the rate limiting step and therefore the amount of the acid sites in this hybrid is insufficient to convert the methanol formed to DME. On the contrary, the CZA-2.7HPW/Ti hybrid is able to convert most of the methanol formed to DME which indicates that it has a sufficient number of acid sites to transform the methanol formed by the CZA. Therefore for the one step DME synthesis over the CZA-xHPW/Ti hybrids its acidity should be balanced with the CZA catalytic function through the HPW loading to maximize the selectivity to DME. Finally it is observed a moderate loss in the DME production with TOS (Table 4) over the 1.7 and 2.7 CZA-xHPW/Ti hybrids that denotes, particularly in the 1.7CZA-xHPW/Ti sample, some kind of deactivation in the acid function of the hybrids. However, this deactivation is much less than that observed in the CZA-HZSM-5 hybrid reference. The deactivation of acid catalysts during DME synthesis is well known in the literature and it is mainly related to the blocking of acid sites by carbonaceous species and/or partial exchange of protons by $\text{Cu}^{2+}/\text{Zn}^{2+}$ [24,71]. The different deactivation rate of the 1.7 and 2.7 CZA-xHPW/Ti hybrids could be related with differences in its surface/bulk acidity ratio derived from their different three-dimensional development, because the deactivation of the surface acid sites by carbonaceous species is faster than the bulk counterparts [72]. However, further studies will be carried out to corroborate this hypothesis and to establish the precise deactivation mechanism of the acid sites present in the CZA-xHPW/Ti hybrids that have been described for the first time as active catalysts for the direct synthesis of DME from syngas.

3. Materials and Methods

3.1. Catalysts Preparation

3.1.1. Cu-ZnO(Al) (CZA) Methanol Synthesis Catalyst

The highly active Cu-ZnO(Al) catalyst (CZA) with optimized composition (Cu/Zn/Al = 68/29/3) was prepared following the methodology proposed as benchmark for Cu-based catalysts and described elsewhere [73]. Hydroxycarbonate precursors were synthesized by co-precipitation from Cu, Zn, Al aqueous nitrate solutions (1M $\text{Cu}(\text{NO}_3)_2 \cdot 2.7\text{H}_2\text{O}$, 99.999%, (Sigma-Aldrich, St. Louis, MO, USA), $\text{Zn}(\text{NO}_3)_2 \cdot 6\text{H}_2\text{O}$, 99.999%, (Sigma-Aldrich, St. Louis, MO, USA), and $\text{Al}(\text{NO}_3)_3 \cdot 9\text{H}_2\text{O}$, 99.997% (Sigma-Aldrich, St. Louis, MO, USA) with Na_2CO_3 1.6M, 99.999%, (Sigma-Aldrich, St. Louis, MO, USA)) under controlled conditions (pH = 6.5, 65 °C). The aged precipitates were filtered and washed several times with deionized water and dried in air at 80 °C for 12 h and calcined under static air at 340 °C for 2 h with a heating rate of 2 °C/min.

3.1.2. H₃PW₁₂O₄₀/TiO₂ Acid Catalysts

A series of supported H₃PW₁₂O₄₀ catalysts (HPW/Ti) were prepared by incipient wetness impregnation on TiO₂ (P25, 54.5 m²/g Alfa Aesar, Ward Hill, MASS, USA). Appropriate amount of H₃PW₁₂O₄₀ (H₃PW₁₂O₄₀·xH₂O (reagent grade, Sigma-Aldrich, St. Louis, MO, USA)) was dissolved on ethanol and impregnated dropwise on the TiO₂ powders. After impregnation, the solids were dried at room temperature for 24 h and thermally treated in an oven using two temperature steps: 50 °C (1 °C/min, 2 h) and subsequent heating at 150 °C (2 °C/min, 2 h). Taking into account that local structure of Keggin units depends on the interaction established between the HPA with the TiO₂ support, we prepared three catalyst samples with H₃PW₁₂O₄₀ loading of 26.3, 30.3 and 41.7 wt % that correspond to 1.4, 1.7 and 2.7 theoretical monolayers respectively, assuming a cross sectional area of 1.13 nm² per Keggin unit [74]. The samples are labelled as xHPW/Ti where x is the theoretical HPAs monolayer (1.4, 1.7 and 2.7).

3.1.3. Bifunctional CZA-xHPW/Ti Hybrid Catalysts

The hybrid catalysts were obtained by physical mixing of xHPW/Ti acid catalysts with CZA calcined powders in an agate mortar with milling during 5 min to form the homogenous mixture of the hybrid catalyst. Prior to mixture, the CZA powders were homogenized in ethanol using a high-performance single-stage dispersing machine (Ultra-Turrax T25 IKA, Staufen, Germany, 14,000 rpm during 20 s, 6 times). The xHPW/Ti/CZA hybrid catalysts was prepared in a mass ratio of 1:2 (w/w) to achieve a theoretical H⁺(HPW)/Cu²⁺(CZA) molar ratio in the hybrids between 0.015 and 0.023. The final catalysts were obtained from the thermal reduction of hybrids under diluted hydrogen flow (2.2 vol % H₂) at 150 °C (2 °C/min) with a subsequent heating at 200 °C (1 °C/min) for 2 h. The hybrids were labelled as CZA-xHPW/Ti where x is the theoretical HPAs monolayer (1.4, 1.7 and 2.7). A bifunctional hybrid catalyst based on the mixing of CZA and HZSM-5 in mass ratio of 1:2 (with excess of acid sites), using the same methodology as commented above, was also prepared as reference catalyst representative of the hybrid formulation most widely used in the bibliography [75,76].

3.2. Physicochemical Characterization

The crystalline structure of xHPW/Ti, CZA and CZA-xHPW/Ti hybrids (in fresh, reduced and used state) were determined from X-ray powder diffraction (XRD) measured using an X'Pert Pro PANalytical (Malvern, Worcs, UK) diffractometer with nickel-filtered Cu K α ₁ radiation ($\lambda = 0.15406$ nm, 45 kV, 40 mA). Crystallite sizes of HPW, CuO, ZnO and Cu⁰ were determined by applying the Debye-Scherrer equation.

Structural information of HPW on xHPW/Ti catalysts was studied by Raman and Diffuse Reflectance Infrared Fourier Transform Spectroscopy (DRIFTS-FTIR). Raman spectra of the xHPW/Ti catalysts were recorded in a Raman spectrometer confocal microscope Renishaw (inVia Raman microscope, Glos, UK). Laser beam in red (785 nm) is used as excitation source with the power set at 300 mW. Raman spectra were collected with a 50 \times objective lens with an acquisition time of 5 s and 10–15 acquisitions. DRIFTS were measured on an infrared spectrometer with MCT-M detector (JASCO FT/IR-6300, Tokyo, Japan). The DRIFTS spectra were obtained with 200 scans and 4 cm⁻¹ resolution at different temperature (25, 150, 200 and 250 °C) purging the cell with He during the experiments. CZA-xHPW/Ti fresh hybrid catalysts were also analysed by DRIFTS at room temperature.

Temperature-programmed reduction (TPR) of CZA catalyst and CZA-xHPW/Ti hybrids were carried out on a semiautomatic PID Eng&Tech (Madrid, Spain) apparatus equipped with a U-shaped quartz reactor and a TC detector. Before reduction the samples (50 mg of pure CZA and 75 mg of hybrids) were treated under He flow (30 mL/min) at 120 °C for 20 min to remove water and other adsorbed contaminants. Reduction profiles were obtained by heating the samples in a 10% H₂/Ar flow (50 NmL/min) from room temperature to 200 °C at a linearly programmed rate of 2 °C/min.

The effluent gas was passed through a cold trap to remove water before measuring the amount of hydrogen consumed during reduction by the thermal conductivity detector.

Specific copper surface areas in reduced CZA catalyst and CZA-xHPW/Ti hybrids were determined from N₂O chemisorption. The reduced samples were treated under diluted N₂O/Ar (2 vol %, 30 mL/min) at room temperature for 5 s. After chemisorption the physisorbed N₂O was removed with He flow (30 mL/min) for 30 min and subsequently reduced under H₂/Ar flow (10 vol % H₂, 50 mL/min) at a heating rate of 10 °C/min up to 200 °C. The hydrogen consumption corresponding to the reduction is equivalent to the amount of consumed N₂O during surface chemisorption. The specific copper surface area was calculated considering a molar stoichiometry of Cu(s)/N₂O = 2 and an average value of 1.47 × 10¹⁹ copper atoms/m² for the surface density of copper metal [77]. The values of copper surface areas in CZA catalyst and CZA-xHPW/Ti hybrids were normalized to the weight of calcined CZA catalysts loaded in the reactor.

Total acidity of xHPW/Ti catalysts and CZA-xHPW/Ti hybrids were determined by temperature programmed desorption of ammonia (NH₃-TPD) which were obtained in an Micromeritics TPD/TPR apparatus (Norcross, GA, USA) coupled with a quadrupole mass spectrometer (OmniStar from Pfeiffer Vacuum, Asslar, Germany). Before chemisorption of ammonia, the samples (with a loading equivalent to 10 mg of HPW) were pre-treated under He flow (30 mL/min) at 240 °C for 20 min and after that, the temperature was lowered to 100 °C under the same He flow. Subsequently, a flow of diluted NH₃ (5 vol %) were introduced at 100 °C until saturation of the sample. After chemisorption, the physisorbed NH₃ was removed with He flow (30 mL/min) for 30 min and subsequently the chemisorbed ammonia was desorbed by heating from 100 to 785 °C at a heating rate of 10 °C/min. The classical detection of NH₃ by TCD was not appropriate for the acidity study on heteropolyacids because desorption of ammonia was accompanied by other products formed from the decomposition of ammonia salts of the heteropolyacids [45]. Therefore the effluent gas was analysed by mass spectrometry (m/z = 16, 18) to follow the NH₃ desorption profiles.

3.3. DME Synthesis from Syngas Tests

Activity tests were performed in a fixed-bed reactor loaded with 0.225 g of hybrid catalysts diluted with SiC (1:3 vol). The hybrids were reduced in situ under hydrogen flow (2.2% H₂/Ar, 50 mL/min) using two temperature steps: 150 °C (2 °C/min) and subsequent heating at 200 °C (1 °C/min) for 2 h. After reduction, the syngas mixture (75 NmL/min, molar composition: 4.5% CO₂, 22.0% CO, 58.8% H₂ and 14.7% N₂) was fed to the reactor. The catalytic tests were conducted at high GHSV (30 L_{syngas} g_{cat}⁻¹ h⁻¹) to achieve low conversions and to exclude the effect of equilibrium and to better visualize the differences in deactivation. Activity was measured at 250 °C and 30 bar maintaining the reaction for 6 h after a catalyst stabilisation time under syngas feed of 1h. The reaction gas products were regularly analysed on-line by GC (Varian 450-GC, Bruker, MASS, USA) with TCD equipped with capillary columns connected in series (QS-bond: CO₂, CH₃OH, DME and H₂O and molecular sieve 5A: H₂, O₂, N₂, CO) gas. The carbon balance was in all tests below 3%. Activity data were reported as CO conversion, product selectivity (DME, methanol and CO₂) and methanol/DME production rate normalized to the weight of hybrid catalyst loaded in the reactor (μmol CH₃OH or DME/g_{cat} min).

CO conversion:

$$X_{CO_x}(\%) = \frac{M_{CO(i)} - M_{CO(f)}}{M_{CO_x(i)}} \cdot 100$$

DME selectivity:

$$S_{DME}(\%) = \frac{M_{DME}}{\sum M_{products}} \cdot 100$$

CH₃OH selectivity:

$$S_{CH_3OH}(\%) = \frac{M_{CH_3OH}}{\sum M_{products}} \cdot 100$$

CO₂ selectivity:

$$S_{CO_2} (\%) = \frac{M_{CO_2}}{\sum M_{products}} \cdot 100$$

DME production rate:

$$R_{pDME} = \frac{M_{DME} (\mu mol)}{m_{cat} (g) \cdot t (min)}$$

CH₃OH production rate:

$$R_{pCH_3OH} = \frac{M_{CH_3OH} (\mu mol)}{m_{cat} (g) \cdot t (min)}$$

where M is the molar flow rate of each component.

4. Conclusions

A series of bifunctional hybrid catalysts based on phosphotungstic acid (H₃PW₁₂O₄₀) supported on TiO₂ combined with Cu-ZnO(Al) catalyst have been prepared, characterised and tested for direct DME synthesis from syngas. The heteropolyacid loading on TiO₂ (from 1.4 to 2.7 theoretical monolayers) affects the dispersion and acid characteristics of the heteropolyacid clusters, resulting in the formation of three-dimensional heteropolyacid nanocrystals with acidity similar to the bulk counterpart when the concentration of the heteropolyacid in the TiO₂ support is higher than 1.7 monolayers. Physical hybridization of supported heteropolyacids with the Cu-ZnO(Al) modifies both the acidic characteristics of the supported heteropolyacids and the copper surface area of the Cu-ZnO(Al) catalyst. The hybrids show a decrease in the copper surface area and the disappearance of the strong acidic sites of pristine HPW nanocrystals, showing all hybrids similar acid sites of weak or medium strength. These changes are related with the migration of water and/or Cu²⁺ or Zn²⁺ species between the supported HPW and Cu-ZnO(Al) during hybridization. The catalytic behaviour of the CZA-xHPW/Ti hybrid catalysts for the direct DME synthesis from syngas (30 bar and 250 °C) depend on their HPW loading. The overall methanol and DME yield on CZA-HPW/Ti hybrids was in all cases lower than the methanol yield achieved on the CZA reference. Only the hybrids with HPW loading higher than 1.7 monolayers are effective for the direct synthesis of DME, reaching the hybrid with 2.7 monolayers (CZA-2.7HPW/Ti) the maximum selectivity for DME (53.0%). These hybrids present three-dimensional HPW structures in which the pseudo-liquid behaviour could occur improving the methanol access to the acid sites. In spite of the high activity of the hybrids, they show a moderate loss in the DME production with TOS that denotes some kind of deactivation of the acidity function under reaction conditions probably related to the blocking of acid sites by carbonaceous species and/or partial exchange of protons by Cu²⁺/Zn²⁺.

Author Contributions: E.M., experiments, investigation, draft preparation; N.M., experiments, investigation, draft preparation; R.G.-L., review; B.P., methodology, review; J.L.G.F., methodology, investigation; R.M.N., conceptualization, methodology, investigation, supervision and writing. All authors have read and agreed to the published version of the manuscript.

Funding: The present investigation was performed within the research programs CTQ2016-76505-C3-1 and PID2019-111219RB-100 supported by the Spanish Ministry of Science, Innovation and Universities. The Autonomous Community of Madrid (CAM) is also gratefully acknowledged for funding BIOTRES-CM (P2018/EMT-4344) project. Elena Millán would like to acknowledge the FPI programme from Spanish Ministry of Science, Innovation and Universities for the research grant.

Conflicts of Interest: The authors declare no conflict of interest. The funders had no role in the design of the study; in the collection, analyses, or interpretation of data; in the writing of the manuscript, or in the decision to publish the results.

References

1. Arcoumanis, C.; Bae, C.; Crookes, R.; Kinoshita, E. The potential of di-methyl ether (DME) as an alternative fuel for compression-ignition engines: A review. *Fuel* **2008**, *87*, 1014–1030. [[CrossRef](#)]

2. Sun, J.; Yang, G.; Yoneyama, Y.; Tsubaki, N. Catalysis chemistry of dimethyl ether synthesis. *ACS Catal.* **2014**, *4*, 3346–3356. [[CrossRef](#)]
3. Semelsberger, T.A.; Borup, R.L.; Greene, H.L. Dimethyl ether (DME) as an alternative fuel. *J. Power Sources* **2006**, *156*, 497–511. [[CrossRef](#)]
4. Jung, J.W.; Lee, Y.J.; Um, S.H.; Yoo, P.J.; Lee, D.H.; Jun, K.-W.; Bae, J.W. Effect of copper surface area and acidic sites to intrinsic catalytic activity for dimethyl ether synthesis from biomass-derived syngas. *Appl. Catal. B Environ.* **2012**, *126*, 1–8. [[CrossRef](#)]
5. Bonura, G.; Cordaro, M.; Spadaro, L.; Cannilla, C.; Arena, F.; Frusteri, F. Hybrid Cu–ZnO–ZrO₂/h-ZSM5 system for the direct synthesis of DME by CO₂ hydrogenation. *Appl. Catal. B Environ.* **2013**, *140–141*, 16–24. [[CrossRef](#)]
6. Behrens, M.; Studt, F.; Kasatkin, I.; Kühl, S.; Hävecker, M.; Abild-Pedersen, F.; Zander, S.; Girgsdies, F.; Kurr, P.; Knief, B.-L.; et al. The active site of methanol synthesis over Cu/ZnO/Al₂O₃ industrial catalysts. *Science* **2012**, *336*, 893–897. [[CrossRef](#)]
7. Grunwaldt, J.D.; Molenbroek, A.M.; Topsøe, N.Y.; Topsøe, H.; Clausen, B.S. In situ investigations of structural changes in Cu/ZnO catalysts. *J. Catal.* **2000**, *194*, 452–460. [[CrossRef](#)]
8. Kanai, Y.; Watanabe, T.; Fujitani, T.; Saito, M.; Nakamura, J.; Uchijima, T. Evidence for the migration of ZnO_x in a Cu/ZnO methanol synthesis catalyst. *Catal. Lett.* **1994**, *27*, 67–78. [[CrossRef](#)]
9. Cai, M.; Palčić, A.; Subramanian, V.; Moldovan, S.; Ersen, O.; Valtchev, V.; Ordonsky, V.V.; Khodakov, A.Y. Direct dimethyl ether synthesis from syngas on copper–zeolite hybrid catalysts with a wide range of zeolite particle sizes. *J. Catal.* **2016**, *338*, 227–238. [[CrossRef](#)]
10. Xie, Q.; Chen, P.; Peng, P.; Liu, S.; Peng, P.; Zhang, B.; Cheng, Y.; Wan, Y.; Liu, Y.; Ruan, R. Single-step synthesis of DME from syngas on cuznal–zeolite bifunctional catalysts: The influence of zeolite type. *RSC Adv.* **2015**, *5*, 26301–26307. [[CrossRef](#)]
11. Takeguchi, T.; Yanagisawa, K.-I.; Inui, T.; Inoue, M. Effect of the property of solid acid upon syngas-to-dimethyl ether conversion on the hybrid catalysts composed of Cu–Zn–Ga and solid acids. *Appl. Catal. A Gen.* **2000**, *192*, 201–209. [[CrossRef](#)]
12. Abu-Dahrieh, J.; Rooney, D.; Goguet, A.; Saih, Y. Activity and deactivation studies for direct dimethyl ether synthesis using CuO–ZnO–Al₂O₃ with NH₄ZSM-5, HZSM-5 or γ-Al₂O₃. *Chem. Eng. J.* **2012**, *203*, 201–211. [[CrossRef](#)]
13. Kozhevnikov, I.V. Sustainable heterogeneous acid catalysis by heteropoly acids. *J. Mol. Catal. A Chem.* **2007**, *262*, 86–92. [[CrossRef](#)]
14. Janik, M.J.; Campbell, K.A.; Bardin, B.B.; Davis, R.J.; Neurock, M. A computational and experimental study of anhydrous phosphotungstic acid and its interaction with water molecules. *Appl. Catal. A Gen.* **2003**, *256*, 51–68. [[CrossRef](#)]
15. Micek-Ilnicka, A. The role of water in the catalysis on solid heteropolyacids. *J. Mol. Catal. A Chem.* **2009**, *308*, 1–14. [[CrossRef](#)]
16. Schnee, J.; Gaigneaux, E.M. Elucidating and exploiting the chemistry of keggin heteropolyacids in the methanol-to-DME conversion: Enabling the bulk reaction thanks to operando raman. *Catal. Sci. Technol.* **2017**, *7*, 817–830. [[CrossRef](#)]
17. Uchida, S.; Inumaru, K.; Misono, M. States and dynamic behavior of protons and water molecules in H₃PW₁₂O₄₀ pseudoliquid phase analyzed by solid-state MAS NMR. *J. Phys. Chem. B* **2000**, *104*, 8108–8115. [[CrossRef](#)]
18. Schnee, J.; Eggermont, A.; Gaigneaux, E.M. Boron nitride: A support for highly active heteropolyacids in the methanol-to-DME reaction. *ACS Catal.* **2017**, *7*, 4011–4017. [[CrossRef](#)]
19. Ladera, R.M.; Ojeda, M.; Fierro, J.L.G.; Rojas, S. TiO₂-supported heteropoly acid catalysts for dehydration of methanol to dimethyl ether: Relevance of dispersion and support interaction. *Catal. Sci. Technol.* **2015**, *5*, 484–491. [[CrossRef](#)]
20. García-López, E.I.; Marci, G.; Krivtsov, I.; Casado Espina, J.; Liotta, L.F.; Serrano, A. Local structure of supported keggin and wells–dawson heteropolyacids and its influence on the catalytic activity. *J. Phys. Chem. C* **2019**, *123*, 19513–19527. [[CrossRef](#)]
21. Alharbi, W.; Kozhevnikova, E.F.; Kozhevnikov, I.V. Dehydration of methanol to dimethyl ether over heteropoly acid catalysts: The relationship between reaction rate and catalyst acid strength. *ACS Catal.* **2015**, *5*, 7186–7193. [[CrossRef](#)]

22. Newman, A.D.; Brown, D.R.; Siril, P.; Lee, A.F.; Wilson, K. Structural studies of high dispersion $H_3PW_{12}O_{40}/SiO_2$ solid acid catalysts. *Phys. Chem. Chem. Phys.* **2006**, *8*, 2893–2902. [CrossRef] [PubMed]
23. Moradi, G.R.; Nosrati, S.; Yariopor, F. Effect of the hybrid catalysts preparation method upon direct synthesis of dimethyl ether from synthesis gas. *Catal. Commun.* **2007**, *8*, 598–606. [CrossRef]
24. García-Trenco, A.; Vidal-Moya, A.; Martínez, A. Study of the interaction between components in hybrid CuZnAl/HZSM-5 catalysts and its impact in the syngas-to-DME reaction. *Catal. Today* **2012**, *179*, 43–51. [CrossRef]
25. Marosi, L.; Escalona Platero, E.; Cifre, J.; Otero Areán, C. Thermal dehydration of $H_{3+x}PV_xM_{12-x}O_{40}\cdot yH_2O$ keggin type heteropolyacids; formation, thermal stability and structure of the anhydrous acids $H_3PM_{12}O_{40}$, of the corresponding anhydrides $PM_{12}O_{38.5}$ and of a novel trihydrate $H_3PM_{12}O_{40}\cdot 3H_2O$. *J. Mater. Chem.* **2000**, *10*, 1949–1955. [CrossRef]
26. Mioč, U.B.; Dimitrijević, R.Ž.; Davidović, M.; Nedić, Z.P.; Mitrović, M.M.; Colomban, P. Thermally induced phase transformations of 12-tungstophosphoric acid 29-hydrate: Synthesis and characterization of PW_8O_{26} -type bronzes. *J. Mater. Sci.* **1994**, *29*, 3705–3718. [CrossRef]
27. Gallardo, R.M.L. Desarrollo de de Wolframio Altamente Activos y Selectivos para la Síntesis de Dimetiléter. Efecto de la Estructura y de la Interacción con el Soporte. Departamento de Química-Física Aplicada, Universidad Autónoma de Madrid. 2013. Available online: https://digital.csic.es/bitstream/10261/80583/1/Ladera%20Gallardo,%20R.M._Tesis_2013.pdf (accessed on 15 September 2020).
28. Alsalme, A.M.; Wiper, P.V.; Khimyak, Y.Z.; Kozhevnikova, E.F.; Kozhevnikov, I.V. Solid acid catalysts based on $H_3PW_{12}O_{40}$ heteropoly acid: Acid and catalytic properties at a gas–solid interface. *J. Catal.* **2010**, *276*, 181–189. [CrossRef]
29. Da Silva, M.J.; de Oliveira, C.M. Catalysis by keggin heteropolyacid salts. *Curr. Catal.* **2018**, *7*, 26–34. [CrossRef]
30. Bielański, A.; Lubańska, A. Ftir investigation on wells–dawson and keggin type heteropolyacids: Dehydration and ethanol sorption. *J. Mol. Catal. A Chem.* **2004**, *224*, 179–187. [CrossRef]
31. Jeantelot, G.; Ould-Chikh, S.; Sofack-Kreutzer, J.; Abou-Hamad, E.; Anjum, D.H.; Lopatin, S.; Harb, M.; Cavallo, L.; Basset, J.-M. Morphology control of anatase TiO_2 for well-defined surface chemistry. *Phys. Chem. Chem. Phys.* **2018**, *20*, 14362–14373. [CrossRef]
32. Agmon, N. The acid test for water structure. *Nat. Chem.* **2016**, *8*, 206–207. [CrossRef] [PubMed]
33. Kulig, W.; Agmon, N. A ‘clusters-in-liquid’ method for calculating infrared spectra identifies the proton-transfer mode in acidic aqueous solutions. *Nat. Chem.* **2013**, *5*, 29–35. [CrossRef] [PubMed]
34. Wang, H.; Agmon, N. Reinvestigation of the infrared spectrum of the gas-phase protonated water tetramer. *J. Phys. Chem. A* **2017**, *121*, 3056–3070. [CrossRef]
35. Bielański, A.; Małecka, A.; Kybelkova, L. Infrared study of the thermal decomposition of heteropolyacids of the series $H_{3+x}PMo_{12-x}V_xO_{40}$. *J. Chem. Soc. Faraday Trans. 1 Phys. Chem. Condens./Phases* **1989**, *85*, 2847–2856. [CrossRef]
36. Hardcastle, F.D. Raman spectroscopy of titania (TiO_2) nanotubular water-splitting catalysts. *J. Ark. Acad. Sci.* **2011**, *65*, 43–48.
37. Lagopati, N.; Tsilibary, E.P.; Falaras, P.; Papazafiri, P.; Pavlatou, E.A.; Kotsopoulou, E.; Kitsiou, P. Effect of nanostructured TiO_2 crystal phase on photoinduced apoptosis of breast cancer epithelial cells. *Int. J. Nanomed.* **2014**, *9*, 3219–3230. [CrossRef]
38. Jagadeeswaraiyah, K.; Kumar, C.R.; Prasad, P.S.S.; Lingaiah, N. Incorporation of Zn^{2+} ions into the secondary structure of heteropoly tungstate: Catalytic efficiency for synthesis of glycerol carbonate from glycerol and urea. *Catal. Sci. Technol.* **2014**, *4*, 2969–2977. [CrossRef]
39. Chai, S.-H.; Wang, H.-P.; Liang, Y.; Xu, B.-Q. Sustainable production of acrolein: Gas-phase dehydration of glycerol over 12-tungstophosphoric acid supported on ZrO_2 and SiO_2 . *Green Chem.* **2008**, *10*, 1087–1093. [CrossRef]
40. Caliman, E.; Dias, J.A.; Dias, S.C.L.; Prado, A.G.S. Solvent effect on the preparation of $H_3PW_{12}O_{40}$ supported on alumina. *Catal. Today* **2005**, *107–108*, 816–825. [CrossRef]
41. Shi, W.; Zhao, J.; Yuan, X.; Wang, S.; Wang, X.; Huo, M. Effects of brønsted and lewis acidities on catalytic activity of heteropolyacids in transesterification and esterification reactions. *Chem. Eng. Technol.* **2012**, *35*, 347–352. [CrossRef]

42. García-López, E.I.; Marci, G.; Pomilla, F.R.; Kirpsza, A.; Micek-Ilnicka, A.; Palmisano, L. Supported $\text{H}_3\text{PW}_{12}\text{O}_{40}$ for 2-propanol (photo-assisted) catalytic dehydration in gas-solid regime: The role of the support and of the pseudo-liquid phase in the (photo)activity. *Appl. Catal. B Environ.* **2016**, *189*, 252–265. [[CrossRef](#)]
43. Caliman, E.; Dias, J.A.; Dias, S.C.L.; Garcia, F.A.C.; de Macedo, J.L.; Almeida, L.S. Preparation and characterization of $\text{H}_3\text{PW}_{12}\text{O}_{40}$ supported on niobia. *Microporous Mesoporous Mater.* **2010**, *132*, 103–111. [[CrossRef](#)]
44. Nakabayashi, H.; Kakuta, N.; Ueno, A. Strong acid sites created on small-sized anatase. *Bull. Chem. Soc. Jpn.* **1991**, *64*, 2428–2432. [[CrossRef](#)]
45. Essayem, N.; Frety, R.; Coudurier, G.; Vedrine, J.C. Ammonia adsorption–desorption over the strong solid acid catalyst $\text{H}_3\text{PW}_{12}\text{O}_{40}$ and its Cs^+ and NH_4^+ salts comparison with sulfated zirconia. *J. Chem. Soc. Faraday Trans.* **1997**, *93*, 3243–3248. [[CrossRef](#)]
46. Southward, B.W.L.; Vaughan, J.S.; Oconnor, C.T. Infrared and thermal analysis studies of heteropoly acids. *J. Catal.* **1995**, *153*, 293–303. [[CrossRef](#)]
47. Grinerval, E.; Rozanska, X.; Baudouin, A.; Berrier, E.; Delbecq, F.; Sautet, P.; Basset, J.-M.; Lefebvre, F. Controlled interactions between anhydrous keggin-type heteropolyacids and silica support: Preparation and characterization of well-defined silica-supported polyoxometalate species. *J. Phys. Chem. C* **2010**, *114*, 19024–19034. [[CrossRef](#)]
48. Agosta, L.; Brandt, E.G.; Lyubartsev, A.P. Diffusion and reaction pathways of water near fully hydrated TiO_2 surfaces from ab initio molecular dynamics. *J. Chem. Phys.* **2017**, *147*, 024704. [[CrossRef](#)]
49. Melián-Cabrera, I.; López Granados, M.; Fierro, J.L.G. Structural reversibility of a ternary $\text{CuO-ZnO-Al}_2\text{O}_3$ ex hydrotalcite-containing material during wet pd impregnation. *Catal. Lett.* **2002**, *84*, 153–161. [[CrossRef](#)]
50. Guil-López, R.; Mota, N.; Llorente, J.; Millán, E.; Pawelec, B.; García, R.; Fierro, J.L.G.; Navarro, R.M. Structure and activity of Cu/ZnO catalysts co-modified with aluminium and gallium for methanol synthesis. *Catal. Today* **2019**. [[CrossRef](#)]
51. Breen, J.P.; Ross, J.R.H. Methanol reforming for fuel-cell applications: Development of zirconia-containing Cu–Zn–Al catalysts. *Catal. Today* **1999**, *51*, 521–533. [[CrossRef](#)]
52. Kuld, S.; Conradsen, C.; Moses, P.G.; Chorkendorff, I.; Sehested, J. Quantification of zinc atoms in a surface alloy on copper in an industrial-type methanol synthesis catalyst. *Angew. Chem. Int. Ed.* **2014**, *53*, 5941–5945. [[CrossRef](#)]
53. García-Trenco, A.; Martínez, A. Direct synthesis of dme from syngas on hybrid CuZnAl/ZSM-5 catalysts: New insights into the role of zeolite acidity. *Appl. Catal. A Gen.* **2012**, *411–412*, 170–179. [[CrossRef](#)]
54. Peng, X.; Toseland, B.; Underwood, R. Studies in surface science and catalysis. In *Catalyst Deactivation*; Bartholomew, G.A.F.C.H., Ed.; Elsevier Science: Amsterdam, The Netherlands, 1997; pp. 175–182.
55. Ordonsky, V.V.; Cai, M.; Sushkevich, V.; Moldovan, S.; Ersen, O.; Lancelot, C.; Valtchev, V.; Khodakov, A.Y. The role of external acid sites of ZSM-5 in deactivation of hybrid CuZnAl/ZSM-5 catalyst for direct dimethyl ether synthesis from syngas. *Appl. Catal. A Gen.* **2014**, *486*, 266–275. [[CrossRef](#)]
56. Sun, J.; Yang, G.; Ma, Q.; Ooki, I.; Taguchi, A.; Abe, T.; Xie, Q.; Yoneyama, Y.; Tsubaki, N. Fabrication of active Cu–Zn nanoalloys on H-ZSM5 zeolite for enhanced dimethyl ether synthesis via syngas. *J. Mater. Chem. A* **2014**, *2*, 8637–8643. [[CrossRef](#)]
57. Flores, J.H.; Pais da Silva, M.I. Acid properties of the hybrid catalyst CuO–ZnO or CuO–ZnO– Al_2O_3 /h-ferrierite: An infrared study. *Coll. Surf. A Physicochem. Eng. Asp.* **2008**, *322*, 113–123. [[CrossRef](#)]
58. Yamamoto, H. From designer lewis acid to designer brønsted acid towards more reactive and selective acid catalysis. *Proc. Jpn. Acad. Ser. B Phys. Biol. Sci.* **2008**, *84*, 134–146. [[CrossRef](#)]
59. Tao, M.; Xue, L.; Sun, Z.; Wang, S.; Wang, X.; Shi, J. Tailoring the synergistic bronsted-lewis acidic effects in heteropolyacid catalysts: Applied in esterification and transesterification reactions. *Sci. Rep.* **2015**, *5*, 13764. [[CrossRef](#)]
60. Karcz, R.; Niemiec, P.; Pamin, K.; Połtowicz, J.; Kryściak-Czerwenka, J.; Napruszewska, B.D.; Michalik-Zym, A.; Witko, M.; Tokarz-Sobieraj, R.; Serwicka, E.M. Effect of cobalt location in keggin-type heteropoly catalysts on aerobic oxidation of cyclooctane: Experimental and theoretical study. *Appl. Catal. A Gen.* **2017**, *542*, 317–326. [[CrossRef](#)]

61. Fyfe, C.A.; Kokotailo, G.T.; Graham, J.D.; Browning, C.; Gobbi, G.C.; Hyland, M.; Kennedy, G.J.; DeSchutter, C.T. Demonstration of contact induced ion exchange in zeolites. *J. Am. Chem. Soc.* **1986**, *108*, 522–523. [[CrossRef](#)]
62. Borbely, G.; Beyer, H.K.; Radics, L.; Sandor, P.; Karge, H.G. Solid-state ion exchange in zeolites: Part iv. Evidence for contact-induced ion exchange between hydrated nay zeolite and metal chlorides. *Zeolites* **1989**, *9*, 428–431. [[CrossRef](#)]
63. Schumann, J.; Lunkenbein, T.; Tarasov, A.; Thomas, N.; Schlögl, R.; Behrens, M. Synthesis and characterisation of a highly active Cu/ZnO: Al catalyst. *ChemCatChem* **2014**, *6*, 2889–2897. [[CrossRef](#)]
64. Chang, C.D. Hydrocarbons from methanol. *Catal. Rev.* **1983**, *25*, 1–118. [[CrossRef](#)]
65. Dadgar, F.; Myrstad, R.; Pfeifer, P.; Holmen, A.; Venvik, H.J. Direct dimethyl ether synthesis from synthesis gas: The influence of methanol dehydration on methanol synthesis reaction. *Catal. Today* **2016**, *270*, 76–84. [[CrossRef](#)]
66. Baltés, C.; Vukojević, S.; Schüth, F. Correlations between synthesis, precursor, and catalyst structure and activity of a large set of CuO/ZnO/Al₂O₃ catalysts for methanol synthesis. *J. Catal.* **2008**, *258*, 334–344. [[CrossRef](#)]
67. Vedage, G.A.; Pitchai, R.; Herman, R.G.; Klier, K. Water promotion and identification of intermediates in methanol synthesis. In Proceedings of the 8th International Congress on Catalysis, Berlin, Germany, 2–6 July 1984; Verlag Chemie: Frankfurt, Germany; International Union of Pure Applied Chemistry: Research Triangle Park, NC, USA, 1984; pp. 47–59.
68. Prašnikar, A.; Pavličič, A.; Ruiz-Zepeda, F.; Kovač, J.; Likozar, B. Mechanisms of copper-based catalyst deactivation during CO₂ reduction to methanol. *Ind. Eng. Chem. Res.* **2019**, *58*, 13021–13029. [[CrossRef](#)]
69. Shikata, S.; Okuhara, T.; Misono, M. Catalysis by hetropoly compounds. Part XXVI. Gas phase synthesis of methyl tert-butyl ether over heteropolyacids. *J. Mol. Catal. A Chem.* **1995**, *100*, 49–59. [[CrossRef](#)]
70. Rykova, A.I.; Burkat, T.M.; Pak, V.N. Hydrate and alcoholate forms of phosphomolybdic heteropolyacid and their formation under conditions of isothermal sorption of water, methanol, and ethanol vapors. *Rus. J. Gen. Chem.* **2003**, *73*, 697–700. [[CrossRef](#)]
71. Dadgar, F.; Myrstad, R.; Pfeifer, P.; Holmen, A.; Venvik, H.J. Catalyst deactivation during one-step dimethyl ether synthesis from synthesis gas. *Catal. Lett.* **2017**, *147*, 865–879. [[CrossRef](#)]
72. Schnee, J.; Gaigneaux, E.M. Lifetime of the H₃PW₁₂O₄₀ heteropolyacid in the methanol-to-DME process: A question of pre-treatment. *Appl. Catal. A Gen.* **2017**, *538*, 174–180. [[CrossRef](#)]
73. Mota, N.; Guil-Lopez, R.; Pawelec, B.G.; Fierro, J.L.G.; Navarro, R.M. Highly active Cu/ZnO–Al catalyst for methanol synthesis: Effect of aging on its structure and activity. *RSC Adv.* **2018**, *8*, 20619–20629. [[CrossRef](#)]
74. Kaba, M.S.; Song, I.K.; Duncan, D.C.; Hill, C.L.; Barteau, M.A. Molecular shapes, orientation, and packing of polyoxometalate arrays imaged by scanning tunneling microscopy. *Inorg. Chem.* **1998**, *37*, 398–406. [[CrossRef](#)] [[PubMed](#)]
75. Kim, J.-H.; Park, M.J.; Kim, S.J.; Joo, O.-S.; Jung, K.-D. Dme synthesis from synthesis gas on the admixed catalysts of Cu/ZnO/Al₂O₃ and ZSM-5. *Appl. Catal. A Gen.* **2004**, *264*, 37–41. [[CrossRef](#)]
76. Mao, D.; Yang, W.; Xia, J.; Zhang, B.; Song, Q.; Chen, Q. Highly effective hybrid catalyst for the direct synthesis of dimethyl ether from syngas with magnesium oxide-modified HZSM-5 as a dehydration component. *J. Catal.* **2005**, *230*, 140–149. [[CrossRef](#)]
77. Bond, G.C.; Namijo, S.N. An improved procedure for estimating the metal surface area of supported copper catalysts. *J. Catal.* **1989**, *118*, 507–510. [[CrossRef](#)]

